# (Sub-)inertial wave boundary turbulence in the Gulf of Valencia

Hans van Haren,[1] Marta Ribó,[2] and Pere Puig[2]

Received 20 December 2012; revised 5 March 2013; accepted 20 March 2013; published 25 April 2013.

[1] The bottom boundary layer above sloping topography can be highly turbulent, even in deep seas. This is demonstrated here using high-resolution 1-Hz sampling temperature sensors that were moored for 5 months every 0.5 m between 6.5 and 61 m above a 572 m deep seafloor promontory on the continental slope off Valencia, Spain. Using these data, turbulence parameters have been estimated. With time and in the vertical, values vary over four orders of magnitude. They have a dominant local inertial period which is modulated by an about 11 day periodicity associated with variations in a baroclinic unstable boundary current. When this current is strong and Eastward, the upslope phase of inertial wave generates convective turbulence which reaches closest to the bottom and therefore can effect sediment dispersal. In late winter, equally strong shear-induced turbulence in 50 m high Kelvin-Helmholtz (K-H) overturns is forced by 0.2 m $s^{-1}$ off/downslope motions, which are preceded by periods of warming of a few 0.01°C before the cooler near-bottom water is suddenly flushed over the promontory into the basin. Such anomalously large K-H overturns occurred 6 times in the investigated winter period.

**Citation:** van Haren, H., M. Ribó, and P. Puig (2013), (Sub-)inertial wave boundary turbulence in the Gulf of Valencia, *J. Geophys. Res. Oceans*, *118*, 2067–2073, doi:10.1002/jgrc.20168.

## 1. Introduction

[2] In the ocean near its boundaries, the Reynolds number $Re = UL/\nu$ is generally so high that motions are quasi-permanently turbulent. In most deep-sea regions, $U = 10^{-1}$ m $s^{-1}$ and $L = 10$ m denote typical velocity and (vertical) length scales, respectively, and $\nu \approx 10^{-6}$ $m^2$ $s^{-1}$ the kinematic viscosity. High values of $Re > 1000$ are also found when the ocean is "stably" vertically stratified in density, notably in large-scale overturns. This makes the ocean an ideal laboratory for studying the transition from sources of motions to their sinks in diapycnal turbulent mixing. The environmental relevance of such studies includes redistribution of nutrients and sediment, which are important for ocean life.

[3] As the ocean is heated at its surface, a mechanical source is needed to mix the heat downward to result in an ocean that is stratified all the way to the bottom [*Munk and Wunsch*, 1998]. The main mechanical source identified to date is dissipation of internal wave energy. Internal waves can have amplitudes of several tens of meters due to the relatively weak restoring force of reduced gravity (multiplying the acceleration of gravity with the relative density difference) [*LeBlond and Mysak*, 1978]. Tides, after interaction with topography, and inertial motions, following geostrophic adjustment on the rotating earth after large-scale disturbances like passing storms, are the main sources of low-frequency internal waves.

[4] Inertial motions generate internal waves that have small vertical scales, so that vertical shear is relatively large, which may lead to shear-induced Kelvin-Helmholtz (K-H) overturning instabilities. However, such turbulent overturning is generally very small in the ocean interior under suppression of the stable stratification. Likewise, the amount of turbulence generated in the boundary layer of a deep flat-bottom ocean is relatively small, because current speeds are in general only a few 0.01 m $s^{-1}$.

[5] In contrast, turbulence parameter values are on average a factor of 100 times larger above sloping bottom topography compared to the ocean interior. Debate has been ongoing whether such enhanced sloping bottom mixing may be sufficient to explain the entire ocean vertical density stratification [*Armi*, 1978; *Garrett*, 1990; *Munk and Wunsch*, 1998]. There are two main processes recognized. First, for relatively large-scale sub-inertial flows, the Ekman rotational effects of bottom friction cause an asymmetry in the boundary layer above a sloping bottom [*Weatherly and Martin*, 1978]. When the interior along-slope flow is "upwelling favorable", it causes the anticlockwise (in the northern hemisphere) deflected near-bottom current to move dense deeper water upslope resulting in enhanced near-bottom stratification which suppresses turbulent exchange. Downwelling favorable flow in opposite direction will create a relatively large, weakly stratified boundary layer which may become convectively unstable. Thus, for steady flows with persistent direction, it is indeed questionable, as advocated by [*Garrett*, 1990], how efficient mixing may be when boundary layers are near homogeneous (as is their

[1]Royal Netherlands Institute for Sea Research (NIOZ), Den Burg, the Netherlands.
[2]Institut de Ciències del Mar, ICM-CSIC. Pg. Marítim de la Barceloneta 37-49, Barcelona, Spain.

Corresponding author: H. van Haren, Royal Netherlands Institute for Sea Research (NIOZ), P.O. Box 59, 1790 AB Den Burg, Netherlands. (hans.van.haren@nioz.nl)


2169-9275/13/10.1002/jgrc.20168

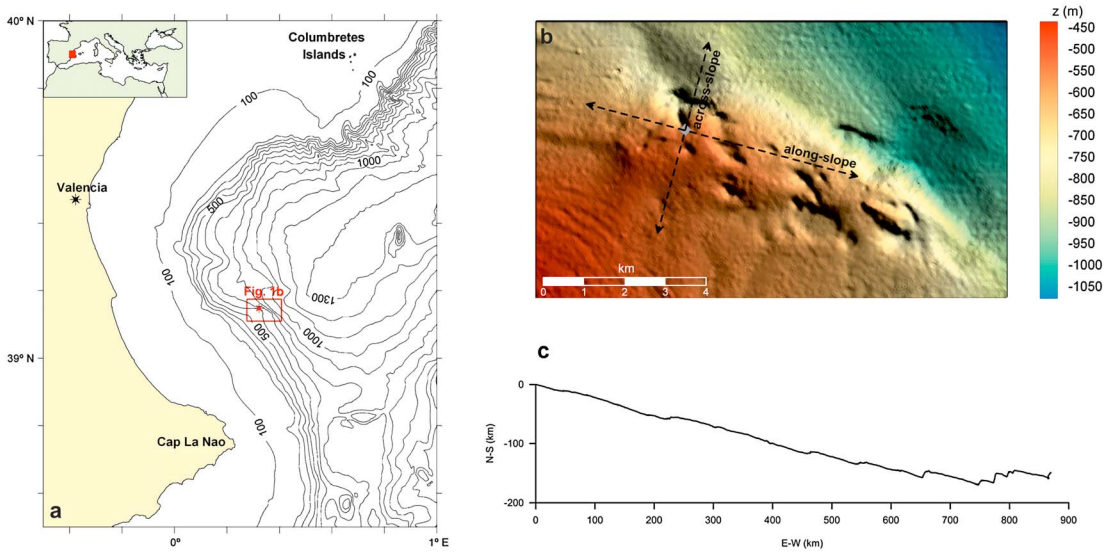


**Figure 1.** Site overview. (a) Bathymetric map of the Gulf of Valencia in the North-Western Mediterranean Sea, showing the study area (rectangle) and the position of the mooring and CTD site (star). (b) Enlargement of rectangle in Figure 1a. Multibeam bathymetric map of the promontory, orientated in a 105–285º direction. Along and across-slope current components are indicated from the mooring (gray diamond). (c) Progressive vector diagram inferred from current measurements at 7 m from the bottom.

common definition): one needs an additional restratifying mechanism for high efficiency. Over time scales of days, the boundary layer may grow up to 100 m from the bottom, but buoyancy forces may balance the frictional Ekman transport so that it shuts down and becomes very slippery [*MacCready and Rhines*, 1993]. On the large scales, the above asymmetry in boundary layer thickness has been observed, e.g., over the northern California shelf [*Lentz and Trowbridge*, 1991]. However, it has also been observed at super-inertial short time scales like those of a tide in the Faeroe-Shetland Channel [*Hosegood and van Haren*, 2004]. Second, internal waves may nonlinearly deform and eventually break at underwater topography creating a vigorously upslope moving turbulent bore [*Vlasenko and Hutter*, 2002; *Klymak and Moum*, 2003]. When they touch the seafloor, such bores dominate sediment resuspension [*Hosegood et al*., 2004]. Including their prefrontal sharpening, they account for 60% of the turbulence generated in a tidal cycle within half an hour as has been observed using high-resolution temperature sensors [*van Haren and Gostiaux*, 2012]. In combination with rapid restratification preceding and following the bore's passage over an internal tide amplitude range about 100 m from the bottom [*van Haren*, 2005], this [internal wave-induced] turbulent mixing is relatively efficient.

[6] In our study, we focus on the Gulf of Valencia (GoV) continental slope, which is located in the Western Mediterranean Sea (Figure 1). The hydrographic structure of this area is characterized by the presence of different water masses (Figure 2). Old Atlantic Waters are found near the surface down to 200 m. Below it, a pool of Western Intermediate Waters (WIW) is formed during wintertime, which is characterized by a relative temperature minimum. Below the WIW, Levantine Intermediate Waters (LIW), characterized by relative temperature and salinity maxima, are centered around 400 m. Deeper down, temperature and salinity decrease again, and the basin is filled with near-homogeneous Western Mediterranean Deep Waters (WMDW). The distribution of suspended sediment concentration (SSC) on the GoV slope is characterized by suspended particle detachments at specific depths forming intermediate nepheloid layers (INLs) and by the development of a bottom nepheloid layer (BNL) below the LIW (Figure 2a) [*Ribó et al*., 2013].

[7] In this paper, we analyze an array of high-resolution temperature sensors moored on the GoV continental slope around the transition between LIW and WMDW. In the absence of strong tides, as is the case here, low-frequency internal waves are dominated by inertial motions. Therefore, the aim of this paper is to characterize the inertial wave boundary turbulence in the GoV and to establish in some detail the different characteristic mixing forms. We are motivated by the possible effects of internal waves and their induced turbulence on sediment dispersal and resuspension that can result in nepheloid layers [e.g., *Cacchione and Drake*, 1986; *McPhee-Shaw*, 2006] developed along the Western Mediterranean continental slope [e.g., *Puig and Palanques*, 1998; *Puig et al*., 2004; *Ribó et al*., 2013].

## 2. Materials and Methods

[8] A total of 110 "NIOZ4" self-contained temperature (T) sensors sampling at 1 Hz, with precision better than 0.001°C [*van Haren et al*., 2009], were mounted at 0.5 m vertical intervals on a nylon-coated steel cable. The lowest sensor was 6.5 m from the bottom. Due to battery problems, every fourth sensor, those that also carried a conductivity sensor, failed most of the observational period. Missing sensor data are interpolated. About 15 m above the upper thermistor a downward looking 300 kHz acoustic Doppler current profiler (ADCP) was mounted sampling at a rate of once

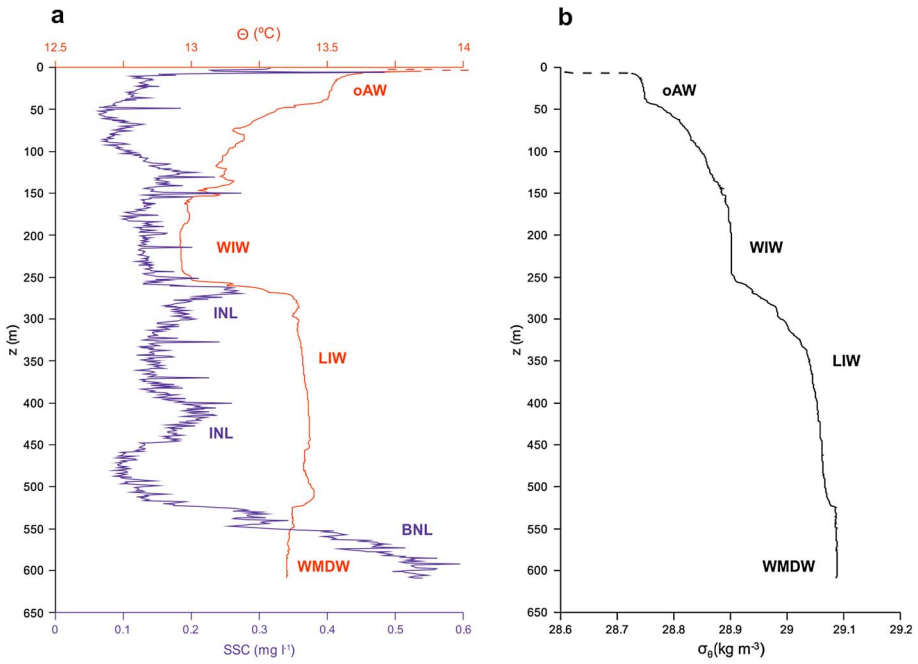


**Figure 2.** CTD observations near the mooring site at the time of instrument retrieval on 3 March 2012. (a) Conservative temperature and SSC vertical profiles. The profiles show the different water masses present in the area (see text for acronyms) and the development of several INLs and a 100 m thick BNL. (b) Density anomaly referenced to the surface.

per 600 s. The instrumented line was moored at 39° 10′N, 0° 20′E, 572 m water depth (Figures 1a and 1b) in October 2011 and recovered in March 2012. This mooring site was located on a promontory protected from fisheries activities. The orientation of the promontory was 105–285º (Figure 1b) and the coordinate system was rotated accordingly to obtain the along-slope (u, positive towards "East") and across-slope (v, positive towards "North": "offslope") current components. The slope orientation is well followed by the general current pattern, as indicated by displacements inferred from progressive vector diagram in Figure 1c. The local bottom slope (not shown) is much steeper (10–15º) than the slightly super-inertial main near-inertial internal wave slope (~1º), under the traditional approximation. However, under near-homogeneous circumstances when the buoyancy frequency $N \sim f$ the inertial frequency, the horizontal component of the Coriolis parameter is no longer negligible and near-inertial waves can propagate under rather steep angles away from near-horizontal [*LeBlond and Mysak*, 1978]. In the open deep Mediterranean, this results in a motion ellipticity that is noncircular [*van Haren and Millot*, 2004].

[9] After correction for slight compressibility effects, the T-data are converted into "conservative" (~potential) temperature data Θ. They are used as tracer for density (ρ) variations following the relation $\delta\rho = -\alpha\delta\Theta$, $\alpha = 0.12 \pm 0.04$ kg $m^{-3}{}^{\circ}C^{-1}$. This relation is established from nearby ship-borne Conductivity-Temperature-Depth (CTD) profile data (Figure 2). α denotes the thermal expansion coefficient under local conditions. Salinity intrusions disturbing this relationship do occur, but are recognizable in detailed computations over short data sections of a few days.

[10] Vertical turbulent eddy diffusivity $K_z$ and turbulent kinetic energy dissipation rate ε are estimated by calculating "overturning" scales using Θ-data and above α. Naturally, such scales cannot be computed during periods when the above density-temperature relationship does not hold. These periods are recognized by layers of different temperature sliding in laterally ("intrusion" periods). They are excluded after visual inspection, as at present no suitable algorithm is established to extract them from the data. For nonintrusion periods, the overturning scales are obtained after reordering every 1-Hz time step potential density (conservative temperature) profile, which may contain inversions, into a stable monotonic profile without inversions [*Thorpe*, 1977, 1987]. After comparing raw and reordered profiles, displacements (d) are calculated necessary for generating the stable profile. A certain threshold applies to disregard apparent displacements associated with instrumental noise in the case of temperature (density) profiles obtained from CTD [*Galbraith and Kelley*, 1996]. In our case, temperature profiles are obtained from a set of ~100 independent sensors and the limiting factor for a threshold is not instrumental noise (which is very low: is $4 \times 10^{-5}{}^{\circ}C$), but rather the remaining temperature shifts after calibration ($<5 \times 10^{-4}{}^{\circ}C$, [*van Haren et al.*, 2009]). Then we estimate,

$$\varepsilon = 0.64 d^2 N^3, \tag{1}$$

where N denotes the buoyancy frequency computed from the reordered profile and the constant follows from empirically relating the overturning scale with the Ozmidov scale $L_O = 0.8d$ [*Dillon*, 1982]. Using $K_z = \Gamma\varepsilon N^{-2}$ and a mixing efficiency for conversion of kinetic into potential energy of $\Gamma = 0.2$ [*Osborn*, 1980], we find,

$$K_z = 0.128 d^2 N. \tag{2}$$

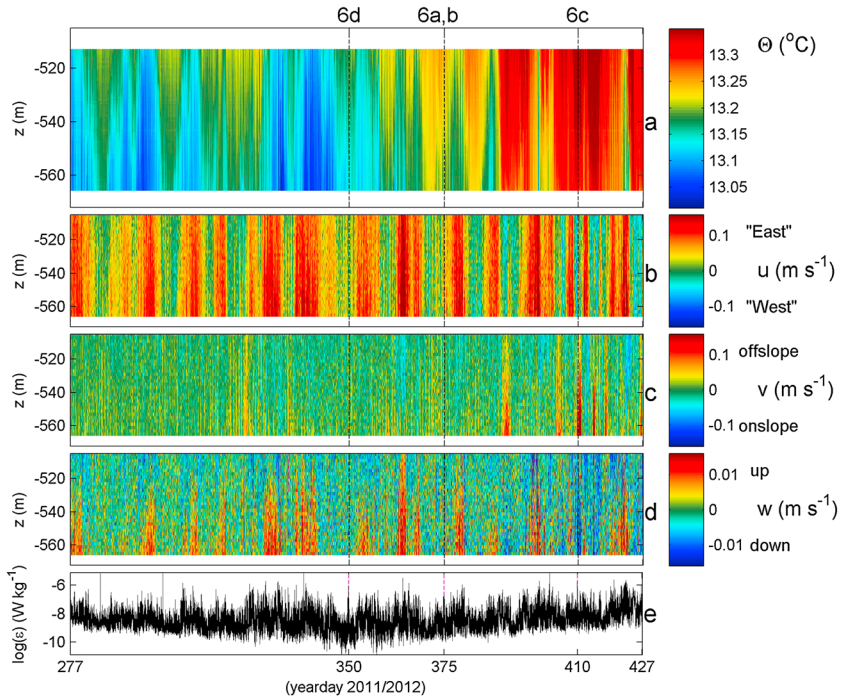


**Figure 3.** Data overview of 150 day time-depth series. Currents are measured using ADCP, whereas temperature, and turbulence parameter estimates are established using high-resolution temperature sensors. (a) Conservative (~potential) temperature. (b) Along-slope current component. (c) Cross-slope current. (d) Vertical current. (e) Vertically averaged (between 6.5 and 59.5 m above the bottom) turbulence dissipation rate inferred from temperature data using the relationship $\delta\rho = -0.12\delta\Theta$ kg m$^{-3}$°C$^{-1}$ (see text). Time in 2012 is +365 days.

## 3. Observations

[11] On the GoV continental slope, watermass variations and currents are dominated by inertial motions and sub-inertial boundary flow (Figures 3a–3d and 4). Sub-inertial kinetic energy is enhanced in a broad band between 5 and 20 day periodicity, with a peak at 11 days (Figure 4). This associates well with the southward extension of the Northern Current, a baroclinic unstable boundary current identified in the northwestern Mediterranean. Previously, its meandering periodicity has been estimated south of the French coast between 2.5 days [*Crepon et al.*, 1982], ~10 days [*Albérola et al.*, 1995], and ~20 days [*Echevin et al.*, 2003]. Here, this associates with turbulence parameter variations having a (broad) inertial periodicity, superposed on a 11 day sub-inertial periodicity, especially clear in the second half of the record (Figure 3e to be compared with Figure 3b; Figure 4). For both periodicities, the phase of strong positive along-slope current shows largest amplitudes. This Eastward current is associated with upslope and bottom-enhanced vertically upward currents, cooler waters, and increased turbulence rates, see e.g. around day 375 for inertial current variations (Figure 5). Although the turbulence parameter estimates over a 150 days long period need to be treated with caution, as no optimal computational filter has yet been established for exclusion of intrusions, the trend of the above periodicities and four orders of magnitude of variation are genuine. Over the 5 months winter period, temperature increases (and density decreases) at the site (Figure 3a). This implies the downslope displacement of LIW presumably by the intrusion of WIW during wintertime (*cf.*, Figure 2). The along-slope current is fairly constant in the vertical (Figure 3b) and nearly always directed towards the east (*cf.*, Figure 1c), but across-slope (Figure 3c) and vertical motions (Figure 3d) are more bottom intensified.

[12] In the second half of the 150 days record, some anomalies to the pattern of (sub-)inertial periodicities occur.

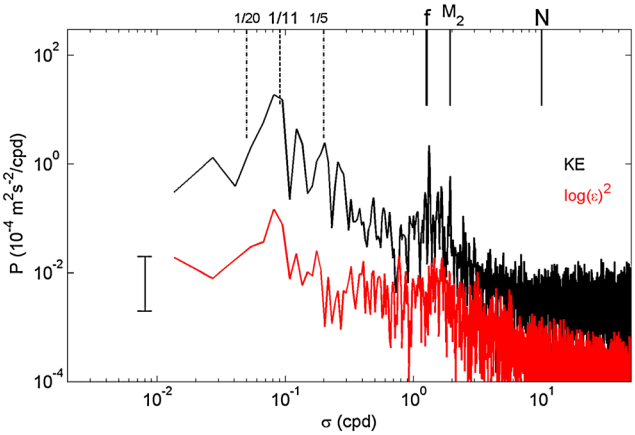


**Figure 4.** Three month long spectra (between days 333 and 425) of ADCP's kinetic energy (black; 550 m) and the logarithm of dissipation rate (red; arbitrary scale in $(W/kg)^2$/cpd; average over the range of [512, 566] m).

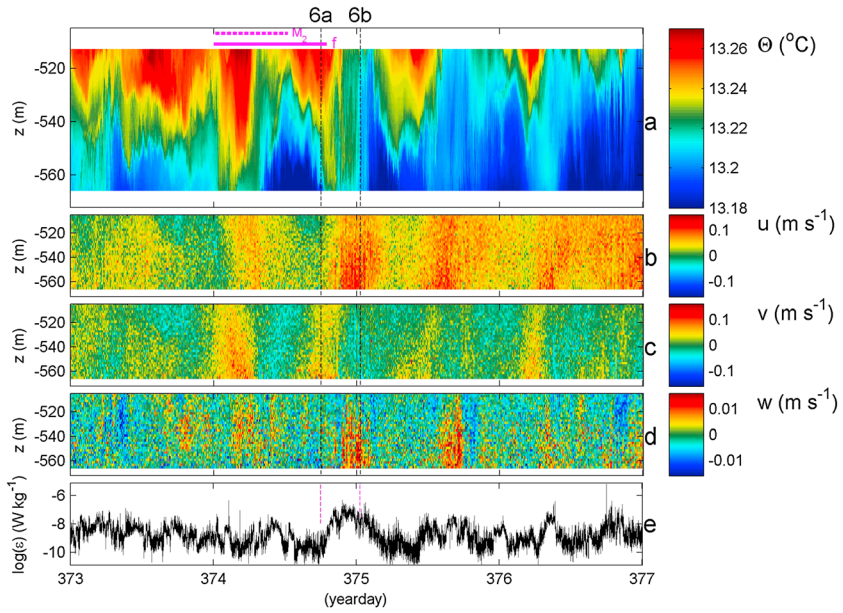


**Figure 5.** As Figure 3, but for four days of detailed observations including two 1-h sample periods of Figure 6. The horizontal purple bars indicate the local inertial (solid) and semidiurnal lunar tidal (dashed) periods. Upper-layer temperature variations show a mix of tidal and inertial periodicities, whereas temperature near the bottom and currents throughout the range mainly show inertial variations.

There are some six major anomalies to the above inertial and sub-inertial periodic turbulent motions (Figure 1c beyond E-W 650 km; Figure 3c during red near-bottom v-current), most in February (days 395–424). These anomalies follow an increase in temperature by a rapid (~0.2 m $s^{-1}$) bottom-intensified offslope motion with relatively strong shear ($|\mathbf{S}| \approx 5 \times 10^{-3}$ $s^{-1} \approx N_{1m}$ computed over small 1-m scales) and some cooling especially near the bottom. Along-slope current amplitude is small, but vertical motions reach amplitudes $< -0.01$ m $s^{-1}$. The sheared cross-slope current (Figure 3c) causes large K-H overturning that can exceed the range of observations (Figure 6c). These observations point at flushing of near-bottom waters into the basin by internal waves across the promontory. This is unusual, as discussed below.

[13] Clearly, distinct differences are observed in boundary layer height and turbulence form, depending on the direction of (internal wave) motions. Two typical 1-h depth-time series (Figures 6a and 6b) of high-resolution temperature sensor data are very different showing stratified perturbations and convective overturning, respectively. In Figure 6a, during an offslope warming phase (*cf.*, Figure 5), the water is vertically stratified in temperature almost throughout the range of sensors and thus stratification approaches the bottom to within 10 m. Small-scale internal waves are visible with periods of about 10 min. Some of these waves are seen to overturn with a typical scale of several meters. In Figure 6b, during an upslope cooling phase (*cf.*, Figure 5), the water is vertically near homogeneous over most of the 53 m observational range. At a fixed depth, temperature is rapidly varying with time, with a ragged strongly turbulent character of vertical motions.

[14] The small-scale overturnings in Figure 6a are turbulent and can be characterized by shear-induced K-H instabilities. The $1–1.5 \times 10^{-3}$ $s^{-1}$ shear-magnitude is partially generated by the large-scale boundary flow, but more so by internal waves. The particular period shows weak positive along-slope and a relatively large (~0.05 m $s^{-1}$) offslope motion. The large turbulent overturning in Figure 6b is found during a period of similar, relatively weak shear ($|\mathbf{S}| \sim 1.5 \times 10^{-3}$ $s^{-1}$ between 530 and 550 m and averaged over an hour), but seems more convectively driven during strong positive along-slope and onslope motion.

[15] Anomalies to the above two typical periods of near-boundary turbulence occur. Under stratified conditions, very large K-H overturns, exceeding the range of sensors, are observed in late winter (Figure 6c). 10-min internal wave shear between 530 and 550 m reaches a magnitude of $9 \times 10^{-3}$ $s^{-1}$. The 1 h and 53 m vertically averaged turbulence parameter values are $< [K_z] > = 1.0 \pm 0.5 \times 10^{-2}$ $m^2$ $s^{-1}$ and $< [\varepsilon] > = 1.5 \pm 0.5 \times 10^{-7}$ W $kg^{-1}$. These values are 100 times larger than those estimated for Figure 6a. Similarly large values as for Figure 6c are found during strong convective overturning periods like that of Figure 6d. For the weakly stratified convection of Figure 6b, about 10 times less dissipation rate is estimated than for Figure 6c.

[16] The time scale of the largest overturns in Figures 6c and 6d is about 1000–1500 s. This is near equal to the (maximum) buoyancy period observed in very thin (<2 m) stratified layers that border the overturns. The shear that (initially) drives such overturns locally varies on the buoyancy scale (reaching $9 \times 10^{-3}$ $s^{-1}$ over 20 m intervals for the period in Figure 6c, so that gradient Richardson number $Ri = N^2/|S|^2 = 0.2 \pm 0.1$). It is superposed on a larger-scale shear (of ~$2 \times 10^{-3}$ $s^{-1}$) such as that of inertial motions and sub-inertial boundary flow.

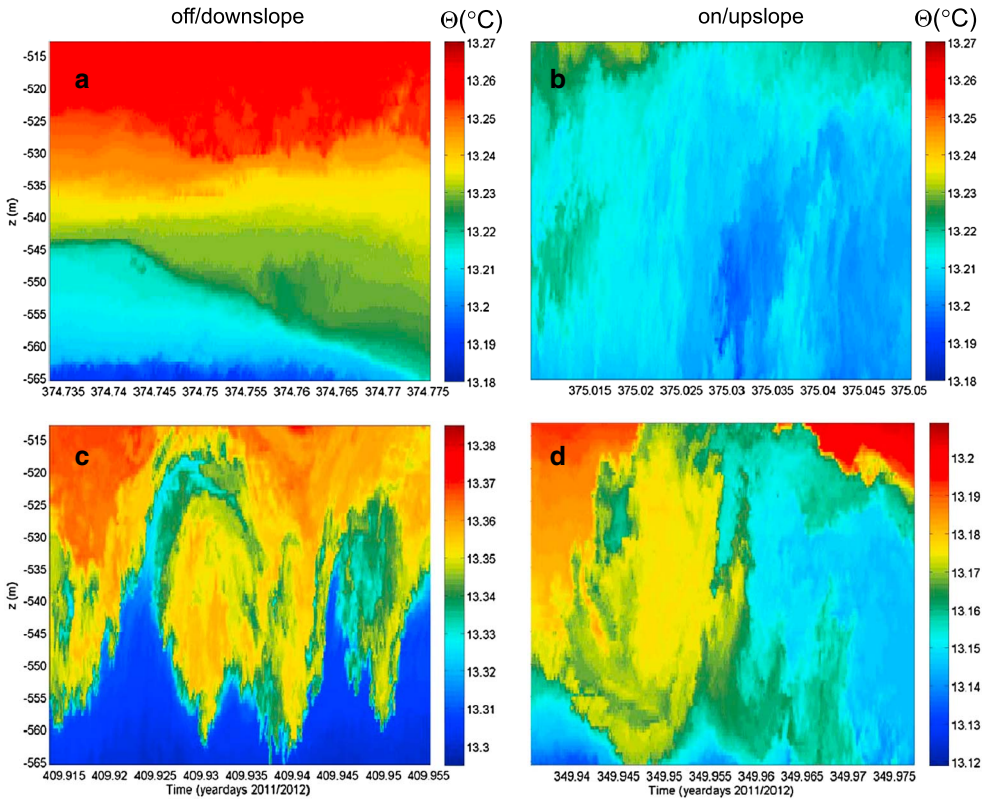


**Figure 6.** Four samples of 1 h time and 53 m vertical range high-precision temperature observations. Note that all panels have a temperature range of 0.09°C, but some differ in absolute values. (a) During typical weak along-slope and offslope flow. (b) During typical strong eastward along-slope and moderate upslope flow. (c) During anomalously strong offslope flow. (d) During anomalously stratified upslope flow.

## 4. Discussion

[17] The more or less 11-day periodic turbulence parameters (in the second half of the observational period; Figures 3e and 4) seem directly associated with the meandering baroclinic unstable boundary current (Figures 3b and 4) and thus with large-scale boundary layer dynamics above sloping bottoms. However, they are not associated with friction on a rotating Earth as they do not comply with Ekman dynamics above sloping bottoms that predict largest turbulence for a downwelling favorable along-slope flow (in this case, Eastward).

[18] Here, the largest turbulence is observed when the eastward along-slope current is accompanied by upslope flow, which moves cold WMDW underneath relatively warmer LIW but simultaneously enlarging the bottom boundary layer as in a wave motion or a bore [*Hosegood et al*., 2004; *Venayagamoorthy and Fringer*, 2012]. This turbulence has a strongly convective apparition and, as far as can be verified with the present data, reaches all the way to the bottom. It can thus be important for resuspension of sediment, prior to dispersal into the basin interior in INLs [*McPhee-Shaw and Kunze*, 2002]. When the along-slope current is weaker, or reversed in direction, and the across-slope flow is directed offslope and downward, the warmer water is stratified close to the bottom. We note that in the latter case, (shear-induced) turbulent diapycnal mixing is still observed, albeit away from the bottom so that sediment is not resuspended but previously suspended matter may still be dispersed into the interior.

[19] The above large-scale process is superseded with smaller-scale variability. On the inertial time scale, of 18.8 h at the present Mediterranean site, largest, convective, turbulence is observed when the along-slope flow is still directed towards the East and upslope, as with the larger scale flow. The vertical motions have inertial periodicity (Figure 5d), especially in near-homogeneous waters, which have proven their convective capability in the very deep Mediterranean [*van Haren and Millot*, 2005; *van Haren and Gostiaux*, 2011]. The superposition of inertial and 11-day periodic motions provides the 0.5–3 h episodes of very large convective turbulence. Such episodes with large, 50 m, overturns have 100 times larger turbulence parameter values than during smaller-scale "quiescent" periods. The latter are typical for open ocean values. Thus, as a single train of large overturns has a duration of typically ~10,000 s, their turbulence can dominate a 11-day period. The varying of turbulence intensity may affect [generation of] short internal waves near the (local) buoyancy frequency.

[20] During offslope flow in late-winter, anomalously large shear-induced overturning result in turbulence that is almost as intense as the convective (upslope flow) turbulence. However, the former is separated from the bottom by intensified stratification around the turbulent cores. Such periods are associated with anomalously large shear and occurred 6 times in slightly more than a month, each time

for the duration of 1–2 h. The accompanying near-bottom intensified offslope flow points at a gravity current, possibly induced by inertial internal wave motion causing WMDW to locally cascade over the promontory. This direct observation of associated large turbulence by a gravity current occurs at speeds of about 0.25 m $s^{-1}$ maximum (15 min average). These turbulent processes might play an important role in the BNL-formation, dispersing the suspended particles. This requires further investigation.

[21] **Acknowledgments.** This research was supported by the project COSTEM (CTM2009-07806). We thank the captain and the crew of the R/V Garcia del Cid for their kind assistance. We thank Martin Laan for all his enthusiastic development of NIOZ-thermistors. We are grateful to the UTM technicians for providing assistance during the data acquisition. M.R. is supported by a FPI grant (Ref. BES-2010-029949) from the Spanish Ministry of Economy and Competitiveness.

## References

Albérola, C., C. Millot, and J. Font (1995), On the seasonal and mesoscale variabilities of the northern current during the PRIMO-0 experiment in the western Mediterranean, *Oceanol. Acta*, *18*, 163–192.

Armi, L. (1978), Some evidence for boundary mixing in the deep ocean, *J. Geophys. Res.*, *83*, 1971–1979.

Cacchione, D. A., and D. E. Drake (1986), Nepheloid layers and internal waves over continental shelves and slopes, *Geo-Mar. Lett.*, *16*, 147–152.

Crepon, M., L. Wald, and J. M. Monget (1982), Low-frequency waves in the Ligurian Sea during December 1977, *J. Geophys. Res.*, *87*, 595–600.

Dillon, T. M. (1982), Vertical overturns: a comparison of Thorpe and Ozmidov length scales, *J. Geophys. Res.*, *87*, 9601–9613.

Echevin, V., M. Crépon, and L. Mortier (2003), Simulation and analysis of the mesoscale circulation in the northwestern Mediterranean Sea, *Annal. Geophys.*, *21*, 281–297.

Galbraith, P. S., and D. E. Kelley (1996), Identifying overturns in CTD profiles, *J. Atmos. Ocean. Tech.*, *13*, 688–702.

Garrett, C. (1990), The role of secondary circulation in boundary mixing, *J. Geophys. Res.*, *95*, 3181–3188.

Hosegood, P., and H. van Haren (2004), Near-bed solibores over the continental slope in the Faeroe-Shetland Channel, *Deep-Sea Res. II*, *51*, 2943–2971.

Hosegood, P., J. Bonnin, and H. van Haren (2004), Solibore-induced sediment resuspension in the Faeroe-Shetland Channel, *Geophys. Res. Lett.*, *31*, L09301, doi:10.1029/2004GL019544.

Klymak, J. M., and J. N. Moum (2003), Internal solitary waves of elevation advancing on a shoaling shelf, *Geophys. Res. Lett.*, *30*, 2045, doi:10.1029/2003GL017706.

LeBlond, P. H., and L. A. Mysak (1978), *Waves in the Ocean*, 602 pp., Elsevier, New York.

Lentz, S. J., and J. H. Trowbridge (1991), The bottom boundary layer over the northern California shelf, *J. Phys. Oceanogr.*, *21*, 1186–1201.

MacCready, P., and P. B. Rhines (1993), Slippery bottom boundary layers on a slope, *J. Phys. Oceanogr.*, *23*, 5–22.

McPhee-Shaw, E. E. (2006), Boundary- Interior Interactions: Reviewing the idea that internal-wave mixing enhances lateral dispersion near continental margins, *Deep-Sea Res. II*, *53*, 42–59.

McPhee-Shaw, E. E., and E. Kunze (2002), Boundary-layer intrusions from a sloping bottom: A mechanism for generating intermediate nepheloid layers, *J. Geophys. Res.*, *107*, C6, 3-1-3-16, doi:10.1029/2001JC000801.

Munk, W., and C. Wunsch (1998), Abyssal recipes II: Energetics of tidal andwind mixing, *Deep-Sea Res. I*, *45*, 1977–2010.

Osborn, T. R. (1980), Estimates of the local rate of vertical diffusion from dissipation measurements, *J. Phys. Oceanogr.*, *10*, 83–89.

Puig, P., and A. Palanques (1998), Nepheloid structure and hydrographic control on the Barcelona continental margin, northwestern Mediterranean, *Mar. Geol.*, *149*, 39–54.

Puig, P., A. Palanques, J. Guillén, and M. El Khatab (2004), Role of internal waves in the generation of nepheloid layers on the northwestern Alboran slope: Implications for continental margin shaping, *J. Geophys. Res.*, *109*, C09011, doi: 10.1029/2004JC002394.

Ribó, M., P. Puig, J. Salat, and A. Palanques (2013), Nepheloid layer distribution in the Gulf of Valencia, northwestern Mediterranean, *J. Mar. Syst.*, *111–112*, 130–138.

Thorpe, S. A. (1977), Turbulence and mixing in a Scottish loch, *Phil. Trans. Roy. Soc. Lond. A*, *286*, 125–181.

Thorpe, S. A. (1987), Transitional phenomena and the development of turbulence in stratified fluids: a review, *J. Geophys. Res.*, *92*, 5231–5248.

van Haren, H. (2005), Details of stratification in a sloping bottom boundary layer of Great Meteor Seamount, *Geophys. Res. Lett.*, *32*, L07606, doi:10.1029/2004GL022298.

van Haren, H., and C. Millot (2004), Rectilinear and circular inertial motions in the Western Mediterranean Sea, *Deep-Sea Res. I*, *51*, 1441–1455.

van Haren, H., and C. Millot (2005), Gyroscopic waves in the Mediterranean Sea, *Geophys. Res. Lett.*, *32*, L24614, doi:10.1029/2005GL023915.

van Haren, H., and L. Gostiaux (2011), Large internal waves advection in very weakly stratified deep Mediterranean waters, *Geophys. Res. Lett.*, *38*, L22603, doi:10.1029/ 2011GL049707.

van Haren, H., and L. Gostiaux (2012), Detailed internal wave mixing observed above a deep-ocean slope, *J. Mar. Res.*, *70*, 173–197.

van Haren, H., M. Laan, D.-J. Buijsman, L. Gostiaux, M.G. Smit, and E. Keijzer (2009), NIOZ3: independent temperature sensors sampling yearlong data at a rate of 1 Hz, *IEEE J.Ocean. Eng.*, *34*, 315–322.

Venayagamoorthy, S. K., and O. B. Fringer (2012), Examining breaking internal waves on a shelf slope sing numerical simulations, *Oceanography*, *25*(2), 132–139, http://dx.doi.org/10.5670/oceanog.2012.48.

Vlasenko, V., and K. Hutter (2002), Numerical experiments on the breaking of solitary internal waves over a slope-shelf topography, *J. Phys. Oceanogr.*, *32*, 1779–1793.

Weatherly, G. L., and P. J. Martin (1978), On the structure and dynamics of the oceanic bottom boundary layer, *J. Phys. Oceanogr.*, *8*, 557–570.